Available online at www.sciencedirect.com
SCIENCE DIRECT®
Synthetic Metals 141 (2004) 179–183
SYNTHETIC METALS
www.elsevier.com/locate/synmet

Multiple Fano effect in charge density wave systems

B. Horovitz [a,*], R. Österbacka [b], Z.V. Vardeny [c]

[a] Department of Physics and Ilze Katz center for nanotechnology, Ben Gurion University of the Negev, Beer-Sheva 84105, Israel
[b] Department of Physics, Åbo Akademi University, Porthansgatan 3, FIN-20500 Turku, Finland
[c] Department of Physics, University of Utah, 114 South 1400 East, Salt Lake City, UT 84112-0830, USA

Received 8 August 2003; accepted 1 September 2003

Abstract

A general framework for analyzing the multiple Fano effect (MFE) in charge density wave (CDW) systems is developed. The MFE occurs when IR active modes have frequencies above the CDW gap and interference between the IR modes and the electronic continuum leads to a series of resonances and anti-resonances. We parameterize the peaks and dips of the absorption by a set of bare frequencies, a pinning parameter and one interaction parameter. We apply this method to recently observed photoinduced absorption spectra of π-conjugated polymer films.

Keywords: Fano resonance; Conjugated polymers; Charge density waves

1. Introduction

The phenomena of multiple Fano Effect (MFE) has been pioneered by Rice [1]. A Fano resonance [2] occurs when a sharp absorption line overlaps with a continuous absorption, resulting in a dip, or anti-resonance, near the absorption peak.

An incommensurate charge density wave (CDW) is of special interest since its very existence leads to new IR active modes. When the frequencies of these modes are above the CDW gap, then Fano interference can occur. Solids with large organic molecules in the unit cell are ideal candidates since the internal molecular vibrations provide high frequency modes. MFE were indeed observed, e.g. in $TEA(TCNQ)_2$ [3], confirming the basic idea presented by Rice [1]. The MFE analysis has also been combined with Raman data leading to quantitative predictions for the various electron–phonon couplings [4].

Of particular interest is the application of MFE to π-conjugated polymers (PCP). Photoinduced charge carriers, e.g. polarons or bi-polarons provide electronic transitions in the IR phonon range, leading to MFE [5]. In this case, the incommensurate CDW corresponds to a localized charge resulting in a space dependent displacement pattern. The rapid development of the quality of PCP through better synthesis and innovative polymers has led to many interesting novel phenomena and applications such as organic light emitting diodes with high luminosity [6], 2D delocalization of charge carriers [7,8] and high mobility field effect transistors [9]. Yet the existence of a continuum electronic state in the charge manifold of such superior polymers has still remained elusive. So far there exist only one definite experimental example of the existence of a continuum band threshold in PCP, namely the Franz–Keldysh-type oscillation measured in the electro-absorption spectrum of a polydiacetylene single crystal [10]. Although photoemission and inverse photoemission measurements were performed in doped and undoped PCP and oligomers [11], these experimental techniques do not have sufficient energy resolution to discern a continuum of electronic states above the discrete excitonic levels.

In the present work, we develop a general framework for analyzing MFE, a phenomena in the non-adiabatic regime. In Section 2, we present the formalism and derive the dominant sharp MFE structure. In Section 3, we analyze photoinduced absorption (PA) spectra of PCP films [5] and show that photoinduced polaron optical transitions to the adjacent electronic band overlap with a series of photoinduced infrared-active vibrations (IRAV), which are known to be formed in PCP when charges are added to the polymer chains. When these conditions are met we observe a series of quantum interference antiresonances (AR) between the two types of excitations, namely the discrete IRAV and the polaron PA band leading to MFE. The Fano-type AR can

* Corresponding author. Tel.: +972-8-6461748; fax: +972-8-6472904.
E-mail address: hbaruch@bgumail.bgu.ac.il (B. Horovitz).

0379-6779/$ – see front matter © 2003 Elsevier B.V. All rights reserved.
doi:10.1016/j.synthmet.2003.09.019

be very well explained by the present theory of MFE even in this non-adiabatic situation. We consider the obtained fit between the data and the model calculation as evidence for the existence of a continuum band above the polaron state in the charge manifold of PCP, justifying the quantitative semiconductor treatments that have been done so far in dealing with organic light emitting diodes and organic field effect transistors.

2. Theoretical framework

We analyze the AR spectrum by a generalization of the amplitude mode (AM) model [12], which has had spectacular success in explaining the resonant Raman scattering (RRS) dispersion as well as photoinduced and doping induced IRAV in PCP [13]. In all of these previous applications of the AM model it has been explicitly assumed that the adiabatic approximation holds true [12]. This was correct since the Raman frequencies are much smaller than the optical gap, and the IRAV frequencies were much smaller than the energy of the photo-induced or doping-induced electronic bands. This approximation, however, does not hold in the case of MFE; we thus have to modify the AM model to allow for non-adiabatic effects.

An important ingredient of the AM model is that all IRAV are interconnected by being coupled to the same electronic operator [1,4,12,13], which is unique to AR in polymers. This makes AR in polymers especially interesting and substantially differs from the more regular Fano-type resonance treatments in other materials [2].

We consider either of the following cases: (i) incommensurate CDW, (ii) commensurate CDW of high order (CDW period > 2 lattice units), and (iii) dimerized CDW, as in PCP, with an additional localized charge. In all of these cases, the displacement pattern $\Delta_n(x)$ for each phonon mode $n = 1, 2, \ldots, N$, is x dependent, either periodic in cases (i) and (ii) or localized in case (iii). In the static situation for each mode $\Delta_n(x) \sim \lambda_n C(x)$ where $C(x)$ is the expectation value of the electronic operator which couples linearly to $\Delta_n(x)$ and λ_n are the electron–phonon couplings. Defining $\lambda = \sum_n \lambda_n$, we have

$$\Delta_n(x) = \frac{\lambda_n}{\lambda}\Delta(x), \tag{1}$$

where $\Delta(x) = \sum_n \Delta_n(x)$ is the collective pattern to which the electrons respond. We allow now small time dependent oscillations, e.g. induced by an external force F. Consequently, each mode acquires a coordinate $\phi_n(t)$, i.e. its displacement pattern is $\Delta_n(x - \phi_n(t))$. We can then define a collective center of mass coordinate $\phi(t)$ via

$$\Delta(x - \phi(t)) = \sum_n \Delta_n(x - \phi_n(t)). \tag{2}$$

Expansion to first order and use of Eq. (1) yields

$$\phi(t) = \sum_n \frac{\lambda_n}{\lambda}\phi_n(t). \tag{3}$$

Next, we wish to evaluate the propagator for the $\phi(t)$ mode in presence of charge pinning, i.e. a restoring force on $\phi(t)$. Pinning is characterized by a single parameter, α, which measures the pinning of the collective translation mode $\phi(t)$. This description of pinning assumes that the charge carriers are sufficiently extended so that individual modes do not couple directly to a pinning center, but only via the collective translation mode. The equations of motion for the modes ϕ_n in the presence of pinning and an external force F are then

$$\left[1 - \left(\frac{\omega}{\omega_n^0}\right)^2\right]\phi_n + \alpha\phi = -F. \tag{4}$$

where ω_n^0 are the bare phonon frequencies. Solution of this equation yields for the collective mode propagator $D_\alpha(\omega)$, defined as the response $\phi = D_\alpha(\omega)F$

$$D_\alpha(\omega) = \frac{D_0(\omega)}{1 - \alpha D_0(\omega)}, \tag{5}$$

where

$$D_0(\omega) = \sum_{n=1}^{N} \frac{\lambda_n}{\lambda} \frac{(\omega_n^0)^2}{\omega^2 - (\omega_n^0)^2 + i\delta_n}, \tag{6}$$

and δ_n are the phonon natural linewidths (in Eq. (4) formally $\delta_n \to +0$). The propagator for the phonons' collective mode $\phi(t)$ in the presence of pinning is therefore $D_\alpha(\omega)$ and is next employed in the treatment of the coupled electron phonon system.

In the MFE regime phonon frequencies overlap with electronic transitions and thus the adiabatic approximation is not valid. However, focusing on a sharp structure in the absorption the random phase approximation (RPA) of Fig. 1 is unique in that it exhibits the sharp structure of $D_\alpha(\omega)$.

We can therefore go beyond the adiabatic approximation by assuming a general response function for the RPA sum (except the first term in Fig. 1 that has no phonons) of the form

$$\begin{aligned} g(\omega) &= -\frac{\omega^2}{E_r^2} \frac{\lambda D_\alpha(\omega) f^2(\omega)}{(1 + 2\lambda D_\alpha(\omega) I_\phi(\omega))} \\ &= -\frac{\omega^2}{E_r^2} \frac{\lambda D_0(\omega) f^2(\omega)}{1 + D_0(\omega)[2\lambda I_\phi(\omega) - \alpha]}, \end{aligned} \tag{7}$$

where $\omega f(\omega)$ is proportional to the electron current coupling to phonons (the first and last bubble in the second and higher terms of Fig. 1) while $I_\phi(\omega)$ is the phonon self mass correction due to the electrons (middle bubbles in Fig. 1); E_r is the

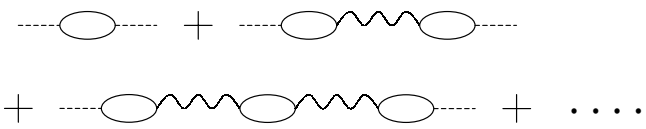

Fig. 1. RPA sum for the conductivity allowing for the sharp structure of the phonon propagator in Eq. (5). The wavy line represents phonons, the dashed line represents the electromagnetic vector potential while the full line represents the electron propagator.

gap for electron–hole excitations, e.g. in presence of a polaron it is the transition from its localized level to the closest continuum. The vertex, $f(\omega)$, and the self mass, I_ϕ, contain, in general, electron–electron interactions. The particular way of exhibiting $f(\omega)$ and $I_\phi(\omega)$ in Eq. (7) is chosen for comparison with the CDW case below. For now, we assume that these functions are smooth on the scale of the fast variation of $D_0(\omega)$, i.e. the spacing between ω_n^0. The phonon contribution to the conductivity is treated within RPA (Fig. 1) since these are the only diagrams where the sharp structure of the collective propagator Eq. (6) is retained—these diagrams are proportional to powers of $D_\alpha(\omega)$. All other diagrams involve integration over phonon lines and the sharp structure is smeared; these terms are represented by additional smooth functions of ω, as $d_1(\omega)$ below.

The total conductance, $\sigma(\omega)$, can be written in the form

$$\sigma(\omega) = \frac{\omega_p^2}{4\pi i\omega}[f(\omega) + d_1(\omega) + g(\omega) - 1], \tag{8}$$

where the term $f(\omega) + d_1(\omega)$ corresponds to the first term in Fig. 1 (without phonons) and -1 is the diamagnetic term. We define

$$c(\omega) = \frac{\lambda\omega^2}{E_r^2} f(\omega), \tag{9}$$

and

$$2\lambda I_\phi(\omega) = 1 + c(\omega) + d_2(\omega), \tag{10}$$

For the CDW case $d_1(\omega) = d_2(\omega) = 0$, but in general I_ϕ can involve terms beyond $c(\omega)$, which are represented by $d_2(\omega)$. In the MFE regime with $\omega > E_r$, all these electronic terms [such as $f(\omega)$; $d_1(\omega)$; $d_2(\omega)$; $c(\omega)$] can be considered as slowly varying on the scale of the spacing between ω_n^0 (which is $\ll E_r$). Since $d_2(\omega)$ appears only in the combination $2\lambda I_\phi(\omega) - \alpha$, we may absorb it into the definition of α, as it is weakly ω dependent.

Collecting terms,

$$\sigma(\omega) = \frac{\omega_p^2}{4\pi i\omega}\left\{f(\omega)\frac{1 + D_0(\omega)[1-\alpha]}{1 + D_0(\omega)[1 + c - \alpha]} - 1\right\} + \text{smooth terms}, \tag{11}$$

and also $c(\omega)$ is taken as a constant c. Hence the sharp structure of $\sigma(\omega)$ can be written as

$$\sigma(\omega) \sim \frac{1 + D_0(\omega)[1-\alpha']}{1 + D_0(\omega)[1 + c_1 - \alpha]}, \tag{12}$$

where $c_1 = \Re(c_1)$ and in general $\alpha' \neq \alpha$ due to the smooth terms. We note that for a single phonon mode Eq. (12) reduces to the form suggested by Fano [2], however, the multi-mode system is not a simple sum of Fano terms.

Peaks of absorption appear at solutions of the equation

$$D_0(\omega) = \frac{-1}{1 - \alpha + c_1}. \tag{13}$$

An interesting feature of this equation is a "product rule" for the N solutions ω_n^ϕ. The denominator in Eq. (12) equation can be written as $\prod_n [\omega^2 - (\omega_n^\phi)^2]/[\omega^2 - (\omega_n^0)^2]$. By comparing values at $\omega = 0$ the product rule is obtained,

$$\prod_{n=1}^{N}\left(\frac{\omega_n^\phi}{\omega_n^0}\right)^2 = \alpha - c_1. \tag{14}$$

We recall that c_1 vanishes for IRAV with $\omega \ll E_r$ [12] so that

$$D_0(\omega) = \frac{-1}{1-\alpha}. \tag{15}$$

We refer to IRAV as the discrete lines at $\omega < E_r$, in contrast to the MFE phenomena at $\omega > E_r$. Dips of absorption (antiresonance) are given by the zeroes of Eq. (12),

$$D_0(\omega) = \frac{-1}{1-\alpha'}, \tag{16}$$

with a product rule for the AR frequencies ω_n^{AR}

$$\prod_{n=1}^{N}\left(\frac{\omega_n^{AR}}{\omega_n^0}\right)^2 = \alpha'. \tag{17}$$

Note that if some ω_n^{AR} are below the gap these are not observable and then the product rule 17 is not useful.

We also recall that for the Raman active modes [12,13]

$$D_0(\omega) = \frac{-1}{1 - 2\tilde{\lambda}}, \tag{18}$$

where $\tilde{\lambda}$ is an interaction parameter (in the absence of electron–electron interactions $\tilde{\lambda} = \lambda$). We summarize all the eigenmodes in Table 1—all of them are determined by the same $D_0(\omega)$ and one additional parameter.

We finally recall the explicit results for the CDW system (in the absence of electron-electron interactions) [1,4,19] at

Table 1
Equations for determining various eigenfrequencies in terms of pinning parameters α, α' and interaction parameters c_1, $\tilde{\lambda}$

Mode and range	Determining equation	Product rule
MFE peaks $\omega_n^\phi > E_r$	$D_0(\omega) = \frac{-1}{1-\alpha+c_1}$	$\prod_{n=1}^{N}\left(\frac{\omega_n^\phi}{\omega_n^0}\right)^2 = \alpha - c_1$
MFE dips (AR) $\omega_n^{AR} > E_r$	$D_0(\omega) = \frac{-1}{1-\alpha'}$	$\prod_{n=1}^{N}\left(\frac{\omega_n^{AR}}{\omega_n^0}\right)^2 = \alpha'$
IRAV $\omega_n^\phi \ll E_r$	$D_0(\omega) = \frac{-1}{1-\alpha}$	$\prod_{n=1}^{N}\left(\frac{\omega_n^\phi}{\omega_n^0}\right)^2 = \alpha$
Resonance Raman $\omega_n^R \ll E_r$	$D_0(\omega) = \frac{-1}{1-2\lambda}$	$\prod_{n=1}^{N}\left(\frac{\omega_n^\phi}{\omega_n^0}\right)^2 = 2\tilde{\lambda}$

E_r is the gap for electron–hole excitation—it may be the transition from valence to conduction band (usually for Raman and IRAV) or a transition between a localized polaron level and the closest continuum as in our PA data.

low temperatures ($T \ll E_r$),

$$f(\omega) = \frac{E_r^2}{\omega^2 y}\arctan\left(\frac{1}{y}\right), \quad \text{if } \omega < E_r$$

$$f(\omega) = \frac{E_r^2}{2\omega^2 y}\left[\ln\left(\frac{1-y}{1+y}\right) + \pi i\right], \quad \text{if } \omega > E_r, \qquad (19)$$

where in both cases $y = \sqrt{|(1 - E_r^2)/\omega^2|}$. Note the complex form for the case $\omega > E_r$.

3. Application to π-conjugated polymers

We have found that AR are quite a generic phenomenon in PA spectra of ordered PCP films, where the polaron $P1$ band overlaps with the IRAVs [5]. There are other examples of photoinduced AR in the PA spectra, such as in polydiacetylene single crystals [14], and other polymer films [15–17] where the AR phenomenon has not been identified or recognized, as well as in charge induced absorption measured in RR-P3HT [18]. We conclude that photoinduced AR are as common as photoinduced IRAV and therefore an appropriate model to describe them is in order.

The poles of Eq. (12) (i.e. Eq. (13)) give MFE peaks in the conductivity (absorption) spectrum. On the other hand, the zeros in Eq. (12) (i.e. Eq. (16)) give the indentations (or AR) in the conductivity spectrum (see Fig. 2). It is thus apparent that the AR are due to the formation of quantum

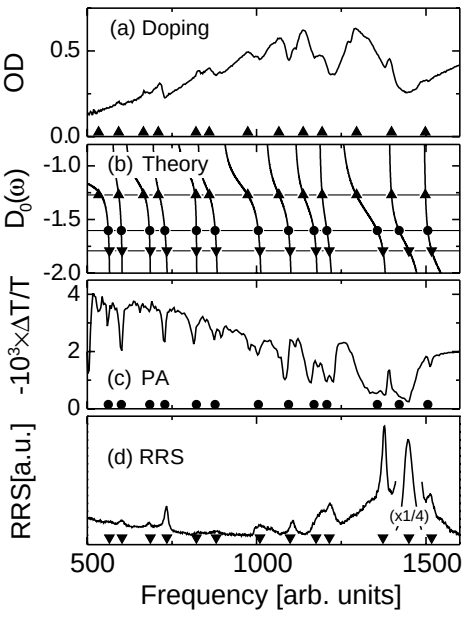

Fig. 2. The measured (lines) and calculated (symbols) for phonon frequencies in (a) doping induced absorption, (c) photoinduced absorption, and (d) resonant Raman spectrum for RRPHT. The fitted propagator $D_0(\omega)$ (with parameters given in Table 2) is shown in (b), where the horizontal lines are obtained using $2\tilde{\lambda} = 0.442$ (RRS, down triangles), $\alpha' = 0.376$ and $c_1 = -0.080$ (ARs, circles) and $\alpha_p = 0.213$ (IRAVs, up triangles). [From Ref. [5]].

Table 2
Fitting parameters obtained for RRPHT

n	ω_n^0 (cm^{-1})	λ_n/λ	δ_n (cm^{-1})	AR(e) (cm^{-1})	AR(c) (cm^{-1})
1	569.5	0.011	15	560	561.8
2	606.5	0.011	15	600	600.3
3	689.1	0.007	17	683	683.0
4	745.2	0.024	25	727	729.0
5	824.5	0.003	35	814	822.0
6	890.3	0.014	30	875	877.8
7	1019.9	0.011	25	1004	1004.8
8	1107.7	0.008	20	1084	1093.8
9	1183.4	0.005	25	1159	1169.4
10	1236.6	0.019	25	1207	1207.6
11	1388.2	0.005	30	1356	1356.0
12	1491.8	0.006	30	1431	1420.7
13	1995.7	0.876	10	1513	1505.4

The bare frequencies ω_n^0, electron–phonon couplings $\lambda_n = \lambda$, natural widths δ_n, together with measured (e) and calculated (c) AR frequencies, respectively, using $2\tilde{\lambda} = 0.442$, $\alpha' = 0.376$, $c_1 = -0.080$ and $\alpha_p = 0.213$.

interference between the phonons and the electron optical transitions in the conductivity spectrum.

To have a more quantitative fit to the experimental PA spectrum of RR-P3HT we used both resonant Raman scattering (RRS) and doping induced absorption spectra (with pinning parameter α_p) of this polymer film to determine the 13 bare phonon frequencies and their corresponding e–p couplings as given in Table 2. Note that the pinning parameter depends on the way charge carriers are produced; a dopant ion is expected to yield a stronger pinning parameter α_p than α for PA charges. We then fit one more parameter (α') to obtain 13 AR frequencies with excellent agreement with the AR data as shown in Table 2.

The 13 coupled phonon modes contain 12 phonons with a relatively weak coupling and a strongly coupled phonon at about 2000 cm^{-1} (the C−C double stretching vibration) with $\lambda_{13} \approx 0.2$; this single mode has ≈0.9 of the overall λ. From these parameters we estimate a superconducting transition temperature $T_c \approx 20$ K [20], which may be reached in the future with clean RRP3AT films in an incommensurate state. This demonstrates the advantage of using the AM model, i.e. the same phonon propagator, which determines the photoinduced AR and IRAV frequencies, also determines the RRS and doping induced IRAV frequencies.

To demonstrate the non-adiabatic effects on the PA spectrum we calculated the conductivity spectrum including the MFE for polarons with low E_r (E_r here is the electronic transition energy within the polaron states) and the corresponding phenomena for high E_r ($\omega < E_r$) which we term as IRAV, as shown in Fig. 3. The calculation uses the CDW form with Eq. (19) assuming a polaron charge that is sufficiently spread to form locally an incommensurate CDW. For these calculations, we used the phonon parameters of RR-P3HT from Table 2. It is seen that when $\omega \ll E_r$, then only IRAV with positive peaks can be observed (Fig. 3(a)); this happens since at $\omega < E_r$ the absorption is anyway weak

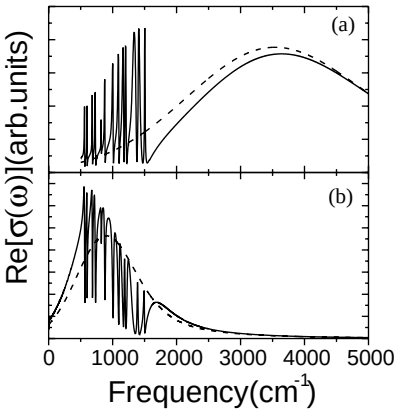

Fig. 3. Calculated PA spectra (solid lines) using the CDW response function with onset 2Δ at: (a) $2\Delta = 2000\,\mathrm{cm}^{-1}$, (b) $2\Delta = 800\,\mathrm{cm}^{-1}$. In both cases, the FWHM of the distribution in Δ is 100%. The electronic CDW PA without phonon contribution is also shown as dashed lines. From [5].

between IRAV frequencies so that a zero factor at the frequencies Eq. (16) is not noticeable. However when E_r is small so that the CDW band overlaps with the IRAV, then quantum interference occur that give rise to MFE in the spectrum (Fig. 3(b)); in this case, the AR are more dominant than the peaks that occur on their high energy side.

4. Conclusions

We have developed a formalism for MFE in CDW systems. These systems are either incommensurate CDW, high order commensurate CDW or dimerized CDW, as in PCP, with an additional localized charge. In all of these systems, we have identified a collective translation mode that couples to the electrons, to an external electric field and to a pinning center. We have shown that a multi-phonon system produces MFE—an interference phenomena in a non-adiabatic regime.

We have applied this analysis to PA spectra of a variety of PCP films and found an excellent agreement. This strongly indicates that in the PA data a continuous absorption band is produced, most likely due to a polaron band [8]. Our analysis, therefore, provides a sensitive tool for identifying a continuous absorption band that overlaps with discrete IRAV.

We have also shown that high frequency modes can be strongly coupled to electrons. In particular in RRPHT we have found that ≈0.9 of the electron–phonon coupling is due to a $2000\,\mathrm{cm}^{-1}$ mode. Such modes are essential for enhancing the superconducting transition temperature within the electron–phonon mechanism. The transition temperatures for superconductivity and for CDW (in the incommensurate case) are comparable when such high frequency modes are strongly coupled [20]. The CDW may be suppressed by increasing interchain coupling and then superconductivity dominates. The MFE analysis presented here is therefore an essential tool for identifying these important strongly coupled high frequency phonons.

In memory of Michael Rice

Michael has been a constant inspiration throughout our work on conducting polymers. Michael's choice of topics and methods, as well as his joyful way of leading dicussions, carried an impact on the whole community.

References

[1] M.J. Rice, Phys. Rev. Lett. 37 (1976) 36.
[2] U. Fano, Phys. Rev. 124 (1961) 1866.
[3] A. Brau, P. Breusch, J.P. Farges, W. Hinz, D. Kuse, Phys. Status Solidi B62 (1974) 615.
[4] B. Horovitz, H. Gutfreund, M. Weger, Phys. Rev. B 17 (1978) 2796.
[5] R. Österbacka, X.M. Jiang, C.P. An, B. Horovitz, Z.V. Vardeny, Phys. Rev. Lett. 88 (2002) 226401.
[6] R.H. Friend, et al., Nature (Lond.) 397 (1999) 121.
[7] H. Sirringhaus, et al., Nature (Lond.) 401 (1999) 685.
[8] R. Österbacka, C.P. An, X.M. Jiang, Z.V. Vardeny, Science 287 (2000) 839.
[9] Z. Bao, A. Dodabalapur, A.J. Lovinger, Appl. Phys. Lett. 69 (1996) 4108;
H. Sirringhaus, N. Tessler, R. Friend, Science 280 (1998) 1741;
B. Crone, et al., Nature (Lond.) 403 (2000) 521.
[10] L. Sebastian, G. Weiser, Phys. Rev. Lett. 46 (1981) 1156.
[11] I.G. Hill, A. Kahn, Z.G. Soos, R.A. Pascal Jr, Chem. Phys. Lett. 327 (2000) 181, and references therein.
[12] B. Horovitz, Solid State Commun. 41 (1982) 729.
[13] E. Ehrenfreund, Z. Vardeny, O. Brafman, B. Horovitz, Phys. Rev. B 36 (1987) 1535.
[14] F.L. Pratt, K.S. Wong, W. Hayes, D. Bloor, J. Phys. C20 (1987) L41;
F.L. Pratt, K.S. Wong, W. Hayes, D. Bloor, J. Phys. D20 (1987) 1361.
[15] Y.H. Kim, D. Spiegel, S. Hotta, A.J. Heeger, Phys. Rev. B38 (1988) 5490.
[16] D. Comoretto, et al., Phys. Rev. B49 (1994) 8059.
[17] H. Johanson, et al., Synth. Metals 101 (1999) 192.
[18] P.J. Brown, H. Sirringhaus, M. Harrison, M. Shkunov, R.H. Friend, Phys. Rev. B63 (2001) 125204.
[19] P.A. Lee, T.M. Rice, P.W. Anderson, Solid State Comm. 14 (1974) 703.
[20] B. Horovitz, Phys. Rev. B16 (1977) 3943.